Korean J. Chem. Eng., 40(7), 1633-1638 (2023)
DOI: 10.1007/s11814-023-1433-z

pISSN: 0256-1115
eISSN: 1975-7220

A first-principles study of B_3O_3 monolayer as potential anode materials for calcium-ion batteries

Mustafa M. Kadhim*,†, Ali Majdi, Safa K. Hachim***,****, Sallalh. Ahmed Abdullaha*****, Taleeb Zedan Taban******, and Ahmed Mahdi Rheima*******

*Medical Laboratory Techniques Department, Al-Farahidi University, Baghdad 10022 Iraq
**Department of Building and Construction Techniques Engineering, Al-Mustaqbal University College, 51001 Hilla, Iraq
***College of Technical Engineering, The Islamic University, Najaf, Iraq
****Medical Laboratory Techniques Department, Al-Turath University College, Iraq, Baghdad
*****The University of Mashreq, Research Center, Baghdad, Iraq
******Laser and Optoelectronics Engineering Department, Kut University College, Kut, Wasit,
*******Department of Chemistry, College of Science, Mustansiriyah University, Baghdad, Iraq
(*Received 9 August 2022 • Revised 11 October 2022 • Accepted 16 November 2022*)

Abstract−Anodic materials with fast kinetics and high capacity are prerequisites for improvement of calcium-ion batteries (CIBs). According to first-principles computations, unique calcium capacity was discovered for B_3O_3 monolayer. Based on findings, Ca atoms can be adsorbed on B_3O_3 surface, and the most stable location is the top of the pore center of B_3O_3 monolayer. Binding energy of B_3O_3 monolayer is relatively high for Ca atoms. In addition, Ca atoms have been shown to more simple diffuse on B_3O_3 surface, and lowest diffusion barrier was 65 meV. A more significant finding is that B_3O_3 monolayer-based nanostructures possess a relatively large capacity of 616.05 mAh/g (as $Ca_{.51}BO$). These results are expected to support illumination mechanism of Ca storage in boron oxide materials with low-dimensional structures and pave the way for design of CIBs. Therefore, we can utilize the B_3O_3 anode-based CIBs as alternatives to normal Ca-ion batteries.

Keywords: Calcium-ion Batteries, B_3O_3 Monolayer, Diffusion Barrier, Anode, Binding Energy

INTRODUCTION

As technology and science continue to advance, there is an increasing need for a large-scale energy storage systems [1-7]. Simultaneously, due to the needs of climate change and resource scarcity, portable and durable batteries have become excellent alternatives for energy storage [8-15]. By employing ionic conductive electrolytes, electrodes of batteries have been separated. An electrochemical process whereby electrode material absorbs energy and releases it through intercalation/deintercalation of alkali metal ions with electrodes is defined as the charging/discharging process of an ion battery [16-25]. Conversion, alloying, and intercalation reactions are the principal mechanisms of frequently inserted and extracted alkaline ions from electroactive materials. Intercalation as basis for early evolution of lithium-ion batteries (LIBs) is the most complete understanding and research to date [26-35]. Since LIBs were first commercialized In 1991, they have been extensively employed in people's daily lives [36]. So far, development of novel LIBs is still an exciting topic. Recent investigations reveal that In_3O_4 [37], B_2P_2 [38], MoC_2 [39], and NP [40] monolayers as anode materials of LIBs possess outstanding performance. Nevertheless, Li-ion batteries suffer more demanding electrodes, low security, and lack of resources [41-45]. To overcome these limitations, research groups are investigating non-lithium-ion batteries (NLIBs). Hence, rechargeable NLIBs with operational safety, natural abundance, and proper negative redox potential have attracted significant interest and are believed as desirable alternatives to conventional Li-ion batteries [46-53]. Meanwhile, the electrochemical performance of NLIB depends to a large extent on specificity of lithium-ion batteries. However, the quality and relatively larger radii of $Al^{3+}/Mg^{2+}/Ca^{2+}/K^{+}/Na^{+}$ ions lead to poor rate capability and capacity retention [54-59]. Therefore, finding appropriate anodes for high-performance NLIBs is critical. Another technology that has proven to be a usable alternative is CIB [60]. In addition to advantages such as safety, abundance and cheapness compared to lithium, calcium has a double charge rating due to its divalent property. In next-generation energy storage systems, CIBs have been demonstrated to deliver more pleasing balance of benefits for usage [61]. Anodic materials with fast kinetics and high capacity are prerequisites for improvement of CIBs. The search for high energy density electrode materials for CIB preparation has become a key issue [62]. With the synthesis of graphene [63,64], which is a two-dimensional material [65-70], a promising energy storage substrate has been provided that allows the free transfer of metal ions between layers due to its high surface-to-mass ratio. To produce 2D cathode materials for LIBs applications, considerable endeavors have been made. For instance, nanostructured MoO_3 (434 mAh/g) [71], MoN_2 (432 mAh/g) [72], ScO_2 (348 mAh/g) [73], and V_2O_5 (274 mAh/g) [74] anode materials were favorably devel-

†To whom correspondence should be addressed.
E-mail: Mustafa_kut88@yahoo.com

oped to offer a very high specific capacity.

Synthesis of a new two-dimensional material based on $RB(OH)_2$ condensation has recently been reported by Stredansky et al. [75]. Employing $H_2B_2O_4$, a six-membered boroxine ring has been formed along with 3 H_2O molecules. In spite of the fact that boroxine layers could readily be characterized in STM analyses, authors recommended that further advancements in synthetic process should be made to decrease the happening of non-six-fold symmetry motifs. Concomitantly, Lin et al. [76] offered a porous boron oxide monolayer with a robust band gap, which is alike to one synthesized by Stredansky et al. [75]. The authors demonstrated that boroxine is perfectly planar with uniform pores of 6.27 Å in diameter and exhibits an indirect wide band gap, which could be used for optoelectronics. From experimental and theoretical points of view, various forms of boron oxide nanomaterials are offered like boron trioxide (B_3O_3), boron suboxide (B_6O), and boron monoxide (B_2O) [76]. In recent years, Stredansky et al. [75] synthesized a new two-dimensional boroxine framework and its stability (porous-hexagonal boron-oxide (ph-BOL)) has been investigated by Lin et al. [76] employing density functional theory (DFT) computations. According to their findings, this is a wide-band gap semiconductor with high dynamic and thermodynamic stability, which is also energetically more stable than other boron-monoxide compounds.

In present work, the feasibility of the B_3O_3 monolayer for Ca storage was evaluated by employing first-principles computations. In addition, it has been concentrated on diffusion and adsorption of Ca atoms on B_3O_3 monolayer where Ca atoms are adsorbed on different sites. Also, principal electrochemical attributes like specific capacity, open-circuit voltage (OCV), diffusion properties, metal adsorption, electronic structures, and geometrical structures have been investigated based on DFT computations.

COMPUTATIONAL DETAILS

All computations were done within DFT formalism employing Perdew-Burke-Ernzerhof function [77] in combination with all electron Pople basis set (6-311+G(d)) as implemented in Gaussian 09 software [78]. By applying empirical dispersion correction in Grimme scheme (DFT-D3), long range interactions have been defined [79, 80]. DFT-D3 dispersion correction has been applied to consider van der Waals interaction between layered system and adatoms. According to the following equation, adsorption stability has been determined by computing Eads of Ca atom on substrate:

$$E_{ad}=(E_{Mg+sub}-E_{sub}-N\times E_{Mg})/N \quad (1)$$

Herein, the number of Ca, energy of an isolated Ca atom, total energy values of pristine substrate (B_3O_3 monolayer) or with adsorbed Ca are represented by N, E_{Ca}, E_{sub}, and E_{Ca+sub} [81].

RESULTS AND DISCUSSION

1. Electronic Attributes and Geometrical Investigation of B_3O_3 Monolayer

At first, hexagonal boron oxide monolayer was optimized as indi-

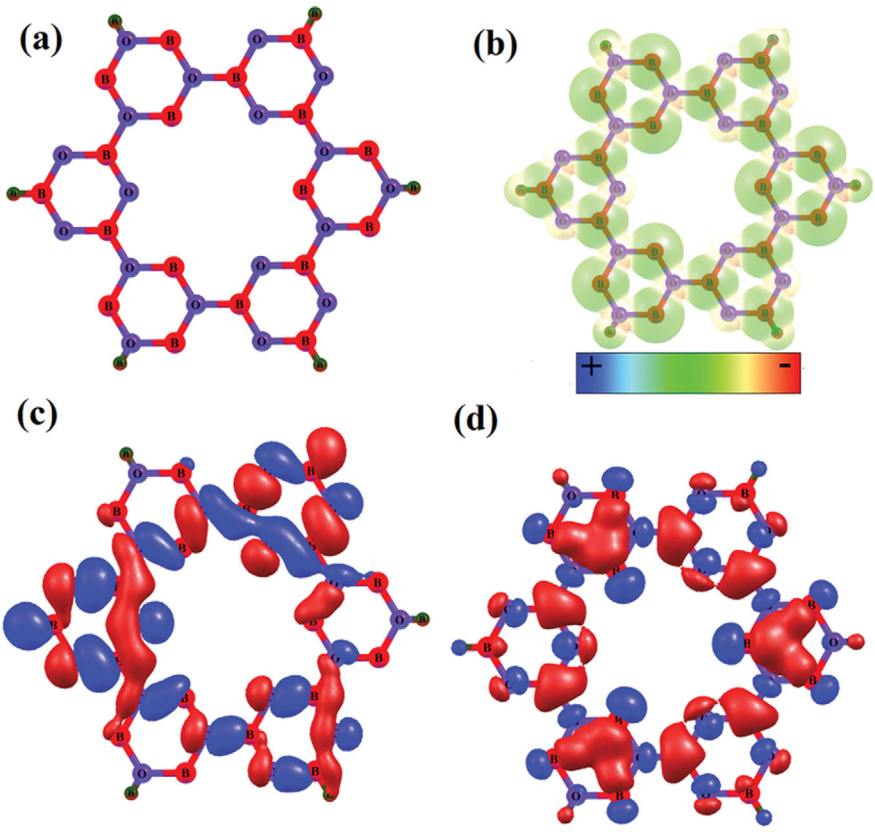

Fig. 1. Optimized geometry (a) Molecular electrostatic potential map, (b) MEP, (c) HOMO and (d) LUMO of B_3O_3 monolayer.

cated in Fig. 1(a). B_3O_3 monolayer includes planar geometry with bond distance of 1.73 Å for B-B, 1.39 Å for B-O, and pore size of 6.28 Å, which are well-consistent with former investigation [76]. According to Fig. 1(b), molecular electrostatic potential (MEP) map indicates surface reactivity of B_3O_3 monolayer in different colors. Herein, neutral area, lower electron density area, electron-rich sites that are covered O atoms because they contain lone pairs of electrons, and electron-deficient sites that are mainly distributed over B atoms are represented by green, yellow, red, and blue, respectively. Lowest unoccupied molecular orbital (LUMO) and highest occupied molecular orbital (HOMO) diagrams are illustrated in Fig. 1(c), (d), indicating LUMO has been mostly distributed over B atoms with −3.36 eV energy. In comparison, HOMO has been mostly localized over O atoms with −7.20 eV energy. According to Hirshfeld charge density analysis, boron carries 0.187 |e| charge and oxygen carries −0.187 |e| charge, which shows stronger bonding nature of B-O (partial ionic character) [76].

2. Adsorbed Atom Diffusion and Adsorption on B_3O_3 Monolayer

The ability to bind Ca within a certain range is a key feature of materials employed as electrodes for Ca storage. Initially, Ca adsorption on B_3O_3 monolayers has been investigated, for which three different feasible adsorption units for Ca were identified. As shown in Fig. 2, seven probable adsorption units have been deemed based on symmetry of structure that are labeled I-VII. At the end of optimizing the full geometry, Ca atoms on site 2 were discovered to move automatically to site 1, which is top of B-B bond in B_3O_3 monolayer pore. Ca atoms on 3, 4 and 5 sites move to site 6, which is in a location in pore center of B_3O_3 monolayer with no energy barriers. This reveals that Ca adsorption at 1, 6 and 7 sites is a spontaneous reaction. Simultaneously, adsorbed Ca atoms on 1, 6, and 7 sites can stay there, excluding for alterations in vertical height in comparison to where they are originated. All of 1, 6 and 7 adsorption sites are stable and can be employed for Ca adsorption that matches with former investigation [82]. Table 1 lists computed findings of

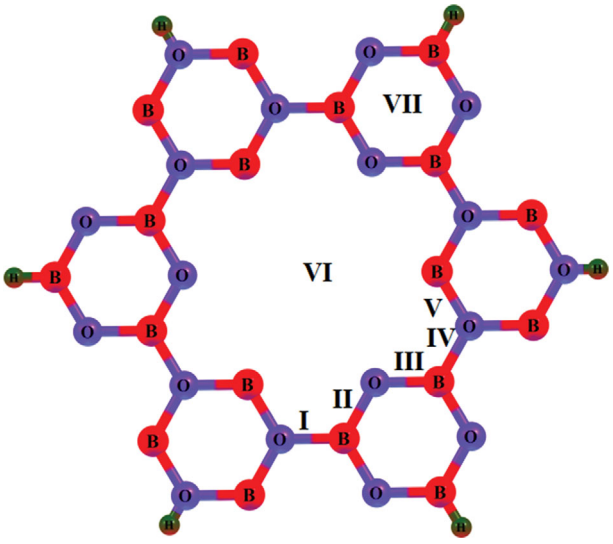

Fig. 2. Top view of the B_3O_3 monolayer and the numbered adsorption sites.

Table 1. E_{ads}, vertical height of Ca top of B_3O_3 monolayer surface (h), distance between an Ca atom and its 3 closest adjacent atoms (d_{Ca}), and total CT from Ca (Q) for 3 stable adsorption sites

Sites	E_{ads} (eV)	h (Å)	d_{Ca} (Å)	Q (e)
1	−0.017	2.76	3.912	0.36
6	−0.644	2.31	3.604	0.238
7	−0.354	2.54	3.623	0.339

E_{ads} for systems, height of adsorption (h), distances between Ca and its three closest-adjacent atoms (d_{Ca}), and CT (Q_{Ca}) of these sites. Also, it indicates that obtained E_{ads} values were negative, which shows Ca adsorption is exothermic in 6 and 7 sites and affirms they are both stable. The most stable adsorption site for a single Ca atom is site 6. Computed E_{ads} of site 6 was −0.644 eV, which is feasible from thermodynamic standpoint. In comparison to site 7, 6 was desirable more energetically, with 0.29 eV higher E_{ads}. E_{ads} of Ca on B_3O_3 surface is lower than that of sodium and lithium, as with adsorption of metals on surface of borophene, arsenene, etc [83-85]. Moreover, h value at the end of relaxation had low value in site 6, which guaranteed strength of Ca and O atoms bonding. Furthermore, there is relatively great CT for both 6 and 7 sites, as summarized in Table 1, which indicates both sites were prevailing and may provide more conductivity to configurations. However, site 6 is more desirable due to considerable CT, low absorption height, and relatively high E_{ads}. Therefore, site 6 has been considered for the rest of the present research.

3. Charge Transfer and Diffusion Energy

Charge density difference at the time of adsorption has been computed to visualize CT of Ca on B_3O_3 monolayer. Aggregation and dissipation of electrons are represented by yellow and blue areas, respectively. Electrons are inclined to gather around more electronegative O atoms, as shown in Fig. 3. Based on Mulligan charge investigation, 0.352 electrons have been transferred during adsorption of Ca at site 6, indicating Ca has been adsorbed on surface of B_3O_3 via chemisorption.

The calculated diffusion energy profiles reveal that Ca ion tends to diffuse from site 7 to 6 via an above of B atom (path A) and B-O bond (path B), which are indicated in Fig. 4(a), (b). A local minimum exists between two saddle points with nearly identical energy barriers. Diffusion energy barrier has been computed about 65 meV, which is significantly lower than other two-dimensional materials, like 0.25 eV for C_2N [86], and 0.29 eV for TiS_3 [87], and also alike to Ca ions diffusion characteristic on surface of arsenene [88]. On condition that Ca ion carried from one adsorption site 7 to 6 from B-O bond, i.e., the B path, there is an energy barrier of 0.37 eV. In every transition state, there is no imaginary frequency according to frequency computation results. Based on the Arrhenius formula [44], diffusion coefficient (D) is in proportion to $\exp(-E_a/k_bT)$, where E_a, k_b, and T are diffusion barrier, Boltzmann constant, and ambient temperature, respectively. It can be concluded that Ca diffusion mobility along A path was approximately more rapid than along B path at ambient temperature. Deformation charge density of O has been computed to better comprehend migration mechanism of Ca on oxygen surface. Oxygen has a sp3 hybrid, and each

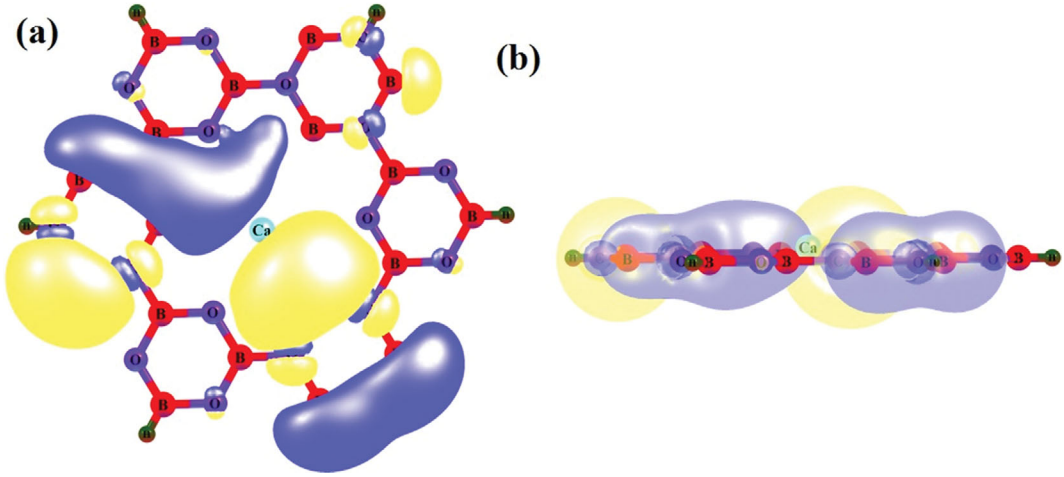

Fig. 3. Difference in charge density between single Ca atoms adsorbed on a monolayer of B_3O_3 at site 4 ((a) top, and (b) side views). Isosurface level has been selected 0.003 e/Å^3. Electron accumulation and depletion are represented by yellow and blue areas, respectively.

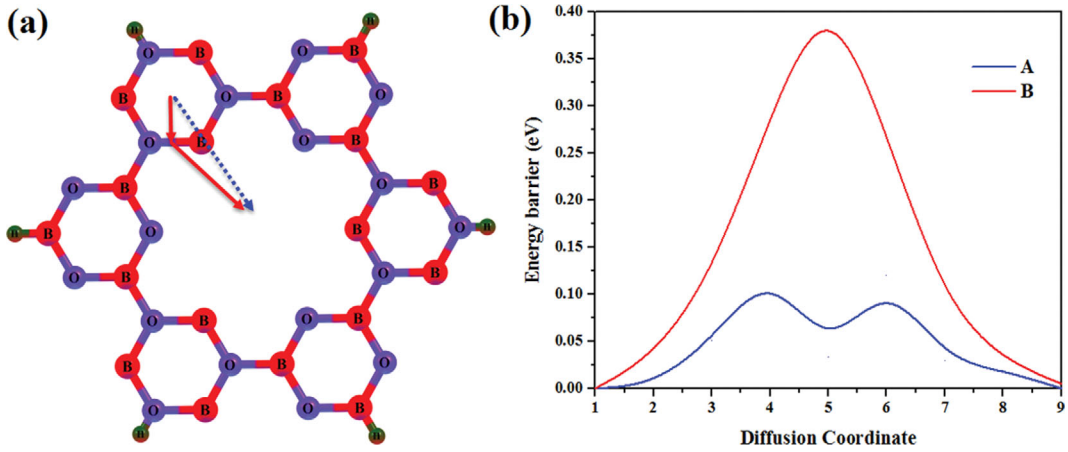

Fig. 4. (a) diffusion paths and (b) energy barriers for Ca diffuse on B_3O_3 monolayer.

O atom has a single pair of electrons that cluster above O atoms. Ca ion must dominate a relatively high electrostatic repulsion force if it diffuses through path B. There is more rapid diffusion mobility and relatively low potential for transition of Ca through path A. Hence, Ca ion diffusion through path A is favorable.

4. The Voltage Profile and Theoretical Specific Capacity

To assess feasibility of electrode materials, ion-specific capacity is another fundamental factor. It was determined whether more than one Ca atom could adsorb on a monolayer of B_3O_3. With a number of adsorbed Ca atoms, average E_{ads} has gradually been enhanced. Adsorption of Ca ions on B_3O_3 monolayer was strongest on the same side, leading to a maximum of 15 adsorbed Ca ions with an average E_{ads} of 1.57 eV. Adsorption of Ca ions can be stable on the surface of B_3O_3 monolayer because E_{ads} is greater than the cohesive energy in the bulk Ca.

According to aforementioned findings, theoretical specific capacity has been determined as below [88]:

$$C = \frac{Z \times x_{max} \times F}{M_{sub}} \quad (2)$$

Herein, Faraday constant, adsorption concentration, number of valence electron (z=2 for Ca), and relative atomic mass of substrate are represented by F, x_{max}, z, and M_{sub}, respectively. The B_3O_3 monolayer can saturate at $Ca_{1.51}BO$ and configurations. Therefore, specific capacities were 616.05 mA h/g ($Ca_{1.51}BO$) for the B_3O_3 monolayer. In this study, specific capacity of graphene-based heterostructures was noted to be significantly higher than that of commercial batteries and to be comparable with specific capacity of a few other anode materials, in which some previously investigated like V_2CO_2/G, $Sc_2C(OH)_2$/G [89], Arsenene/G [88], ZrS_2/G [90], $Ti_2C(OH)_2$/G, Ti_2CO_2/G, and Ti_2CF_2/G [91]. The ΔG value of Ca adsorption on the B_3O_3 surface was calculated. The ΔG value was decreased by increasing the number adsorption of Ca, when the My number was increased from 1 to 4 the ΔG value was decreased from −8.21 to −3.47 kJ mol^{-1}, respectively. However, the system interaction is favorable for the Gibbs free energy change, and the stronger interaction causes a more negative Gibbs free energy change.

For rechargeable batteries, open-circuit voltage (OCV) is the other main factor. By computation of average voltage (U), OCV can be assessed as below [92]:

$$U_{ave} = \frac{(E_{sub} + xE_{Mg} - E_{Mg+sub})}{2xe} \quad (3)$$

where, energy per atom in bulk Ca crystal, total energy of substrate adsorbed with x Ca atoms, and total energy of substrate are represented by E_{Ca}, E_{Ca+sub}, and E_{sub}. The average electrode potentials of B_3O_3 monolayer were 0.142 V. These electrode potentials are generally comparable with commercial anodes for LIBs, like 1.5 V for TiO_2 [93] and 0.11 V for graphite [94]. Both lower OCV and desirable theoretical specific capacity reveal that B_3O_3 monolayer can be an appropriate electrode material. To the best of our knowledge, considerable increase in volume of Ca ion adsorption usually disrupts the useful life of electrode material. Hence, alteration of lattice constant has a critical effect on evaluation of structural integrity for electrode material. Lattice change rate was 7.22% for B_3O_3 monolayer. This shows B_3O_3 monolayer is favorably stable as anode material of CIBs.

CONCLUSIONS

The potential of B_3O_3 monolayer to employ as an anode material for CIBs was investigated based on first-principles computations. The B_3O_3 monolayer was investigated for the first time as an anode material for Ca-ion batteries in this work. According to results, adsorbed Ca on a monolayer of B_3O_3 has stability with 65 meV diffusion barrier, which reveals charge-discharge rate is relatively rapid. In comparison to various commercial batteries, B_3O_3 includes higher theoretical specific capacity (616.05 mA h/g), superior electrical conductivity, and more stability. The full adsorption of Ca onto the B_3O_3 monolayer results in a very low OCV of ~0.142 V, which shows that the operating voltage for full-cells is high. These results are expected to help comprehend the mechanism of two-dimensional B_3O_3 monolayer energy storage, and supply a practical guide to logical design of promising anodes. Finally, a feasible and efficient strategy was developed to design light two-dimensional anode materials in batteries.

SUPPORTING INFORMATION

Additional information as noted in the text. This information is available via the Internet at http://www.springer.com/chemistry/journal/11814.

REFERENCES

1. Z. P. Cano, D. Banham, S. Ye, A. Hintennach, J. Lu, M. Fowler and Z. Chen, *Nature Energy*, **3**, 279 (2018).
2. E. Bullich-Massagué, F.-J. Cifuentes-García, I. Glenny-Crende, M. Cheah-Mañé, M. Aragüés-Peñalba, F. Díaz-González and O. Gomis-Bellmunt, *Appl. Energy*, **274**, 115213 (2020).
3. B. K. Saikia, S. M. Benoy, M. Bora, J. Tamuly, M. Pandey and D. Bhattacharya, *Fuel*, **282**, 118796 (2020).
4. M. Mortazavi, C. Wang, J. Deng, V. B. Shenoy and N. V. Medhekar, *J. Power Sources*, **268**, 279 (2014).
5. Y. Liu, J. Li, W. Li, Y. Li, F. Zhan, H. Tang and Q. Chen, *Int. J. Hydrogen Energy*, **41**, 10354 (2016).
6. T. Zhang, L. Yang, C. Zhang, Y. Feng, J. Wang, Z. Shen, Q. Chen, Q. Lei and Q. Chi, *Mater. Horizons*, **9**, 1273 (2022).
7. M. Yang, C. Li, Y. Zhang, Y. Wang, B. Li, D. Jia, Y. Hou and R. Li, *Appl. Therm. Eng.*, **126**, 525 (2017).
8. X. Feng, M. Ouyang, X. Liu, L. Lu, Y. Xia and X. He, *Energy Storage Mater.*, **10**, 246 (2018).
9. F. Schipper and D. Aurbach, *Russ. J. Electrochem.*, **52**, 1095 (2016).
10. J. L. Shi, D. D. Xiao, M. Ge, X. Yu, Y. Chu, X. Huang, X. D. Zhang, Y. X. Yin, X. Q. Yang and Y. G. Guo, *Adv. Mater.*, **30**, 1705575 (2018).
11. J. Xu, Y. Dou, Z. Wei, J. Ma, Y. Deng, Y. Li, H. Liu and S. Dou, *Adv. Sci.*, **4**, 1700146 (2017).
12. S. Hu, Y. Yong, Z. Zhao, R. Gao, Q. Zhou and Y. Kuang, *Int. J. Hydrogen Energy*, **46**, 21994 (2021).
13. A. Y. Galashev, K. A. Ivanichkina, A. S. Vorob'ev, O. R. Rakhmanova, K. P. Katin and M. M. Maslov, *Int. J. Hydrogen Energy*, **46**, 17019 (2021).
14. A. I. Kamisan, T. I. Tunku Kudin, A. S. Kamisan, A. F. Che Omar, M. F. Mohamad Taib, O. H. Hassan, A. M. M. Ali and M. Z. A. Yahya, *Int. J. Hydrogen Energy*, **47**, 8630 (2022).
15. T. Wei, Z. Wang, M. Zhang, Q. Zhang, J. Lu, Y. Zhou, C. Sun, Z. Yu, Y. Wang and M. Qiao, *Mater. Today Commun.*, **31**, 103518 (2022).
16. D. Rao, L. Zhang, Z. Meng, X. Zhang, Y. Wang, G. Qiao, X. Shen, H. Xia, J. Liu and R. Lu, *J. Mater. Chem. A*, **5**, 2328 (2017).
17. V. Shukla, R. B. Araujo, N. K. Jena and R. Ahuja, *Nano Energy*, **41**, 251 (2017).
18. C. Zhang, Y. Ma, X. Zhang, S. Abdolhosseinzadeh, H. Sheng, W. Lan, A. Pakdel, J. Heier and F. Nüesch, *Energy Environ. Mater.*, **3**, 29 (2020).
19. H. Jiang, W. Shyy, M. Liu, L. Wei, M. Wu and T. Zhao, *J. Mater. Chem. A*, **5**, 672 (2017).
20. F. Li, Y. Qu and M. Zhao, *J. Mater. Chem. A*, **4**, 8905 (2016).
21. S. Ullah, P. A. Denis and F. Sato, *New J. Chem.*, **42**, 10842 (2018).
22. X. Zhang, Y. Tang, F. Zhang and C. S. Lee, *Adv. Energy Mater.*, **6**, 1502588 (2016).
23. X. Tong, F. Zhang, B. Ji, M. Sheng and Y. Tang, *Adv. Mater.*, **28**, 9979 (2016).
24. B. Ji, F. Zhang, X. Song and Y. Tang, *Adv. Mater.*, **29**, 1700519 (2017).
25. S. Mu, Q. Liu, P. Kidkhunthod, X. Zhou, W. Wang and Y. Tang, *National Sci. Rev.*, **8**, nwaa178 (2021).
26. J. B. Goodenough and K.-S. Park, *J. Am. Chem. Soc.*, **135**, 1167 (2013).
27. A. Yoshino, K. Sanechika and T. Nakajima, Google Patents (1987).
28. Y. Nishi, *J. Power Sources*, **100**, 101 (2001).
29. D. Deng, M. G. Kim, J. Y. Lee and J. Cho, *Energy Environ. Sci.*, **2**, 818 (2009).
30. B. Dunn, H. Kamath and J.-M. Tarascon, *Science*, **334**, 928 (2011).
31. D. Deng, *Energy Sci. Eng.*, **3**, 385 (2015).
32. C. Zhao, M. Xi, J. Huo and C. He, *Phys. Chem. Chem. Phys.*, **23**, 23219 (2021).
33. X. Chen, L. Li, Y. Shan, D. Zhou, W. Cui and Y. Zhao, *J. Energy Chem.*, **70**, 502 (2022).
34. Y. Shan, L. Li, X. Chen, S. Fan, H. Yang and Y. Jiang, *ACS Energy Lett.*, **7**, 2289 (2022).
35. H. Li, Y. Zhang, C. Li, Z. Zhou, X. Nie, Y. Chen, H. Cao, B. Liu, N. Zhang and Z. Said, *Korean J. Chem. Eng.*, **39**, 1107 (2022).
36. Y. Nishi, *Chem. Rec.*, **1**, 406 (2001).

37. L. Shao, X. Duan, Y. Li, Q. Yuan, H. Ye and P. Ding, *J. Phys. Chem. C*, **123**, 30213 (2019).
38. H. Lin, G. Liu, L. Zhu, Z. Zhang, R. Jin, Y. Huang and S. Gao, *Appl. Surf. Sci.*, **544**, 148895 (2021).
39. Y. Yu, Z. Guo, Q. Peng, J. Zhou and Z. Sun, *J. Mater. Chem. A*, **7**, 12145 (2019).
40. Z. Cheng, X. Zhang, H. Zhang, J. Gao, H. Liu, X. Yu, X. Dai, G. Liu and G. Chen, *Appl. Surf. Sci.*, **547**, 149209 (2021).
41. A. Opitz, P. Badami, L. Shen, K. Vignarooban and A. M. Kannan, *Renew Sust. Energy Rev.*, **68**, 685 (2017).
42. J.-M. Tarascon and M. Armand, Materials for sustainable energy: a collection of peer-reviewed research and review articles from Nature Publishing Group, World Scientific, 171 (2011).
43. R. Jiang, M. Jiang, Z. Huang, J. Wang, Y. Kuang and C. Fu, *Int. J. Hydrogen Energy*, **45**, 14940 (2020).
44. G. Lei, Z. Wang, J. Xiong, S. Yang, H. Xu, Z. Lan and H. Gu, *Int. J. Hydrogen Energy*, **45**, 10257 (2020).
45. Y. Xu, X. Chen, H. Zhang, F. Yang, L. Tong, Y. Yang, D. Yan, A. Yang, M. Yu and Z. Liu, *Int. J. Energy Res.*, **46**, 19615 (2022).
46. W. Li, Q. Song, M. Li, Y. Yuan, J. Zhang, N. Wang, Z. Yang, J. Huang, J. Lu and X. Li, *Small Methods*, **5**, 2100444 (2021).
47. H. Shan, J. Qin, Y. Ding, H. M. K. Sari, X. Song, W. Liu, Y. Hao, J. Wang, C. Xie and J. Zhang, *Adv. Mater.*, **33**, 2102471 (2021).
48. Y.-J. Lei, Z.-C. Yan, W.-H. Lai, S.-L. Chou, Y.-X. Wang, H.-K. Liu and S.-X. Dou, *Electrochem. Energy Rev.*, **3**, 766 (2020).
49. G. Wang, X. Bi, H. Yue, R. Jin, Q. Wang, S. Gao and J. Lu, *Nano Energy*, **60**, 362 (2019).
50. Z. Liu, S. Liu and S. Er, *Int. J. Hydrogen Energy*, **44**, 16803 (2019).
51. J. Zhao, J. Gao, W. Li, Y. Qian, X. Shen, X. Wang, X. Shen, Z. Hu, C. Dong and Q. Huang, *Nat. Commun.*, **12**, 1 (2021).
52. L. Yang, Q. Dai, L. Liu, D. Shao, K. Luo, S. Jamil, H. Liu, Z. Luo, B. Chang and X. Wang, *Ceram. Int.*, **46**, 10917 (2020).
53. X. Wu, C. Li, Z. Zhou, X. Nie, Y. Chen, Y. Zhang, H. Cao, B. Liu, N. Zhang and Z. Said, *Int. J. Adv. Manuf. Technol.*, **117**, 2565 (2021).
54. Y. Wang, R. Chen, T. Chen, H. Lv, G. Zhu, L. Ma, C. Wang, Z. Jin and J. Liu, *Energy Storage Mater.*, **4**, 103 (2016).
55. H. Huang, R. Xu, Y. Feng, S. Zeng, Y. Jiang, H. Wang, W. Luo and Y. Yu, *Adv. Mater.*, **32**, 1904320 (2020).
56. X. Wu, D. P. Leonard and X. Ji, *Chem. Mater.*, **29**, 5031 (2017).
57. B. J. Cid, A. N. Sosa, Á. Miranda, L. A. Pérez, F. Salazar, A. I. Mtz-Enriquez and M. Cruz-Irisson, *Int. J. Hydrogen Energy*, **47**, 41310 (2022).
58. M. Wang, C. Jiang, S. Zhang, X. Song, Y. Tang and H.-M. Cheng, *Nat. Chem.*, **10**, 667 (2018).
59. Z. Li, X. He, C. Zhang, X. Wang, S. Zhang, Y. Jia, S. Feng, K. Lu, J. Zhao and J. Zhang, *Nat. Commun.*, **13**, 1 (2022).
60. M. V. Sofianos, S. Randall, M. Paskevicius, K.-F. Aguey-Zinsou, M. R. Rowles, T. D. Humphries and C. E. Buckley, *J. Alloys Compd.*, **819**, 153340 (2020).
61. A. F. Sammells and B. Schumacher, *J. Electrochem. Soc.* (United States), **133**, 235 (1986).
62. S. Mukherjee and G. Singh, *ACS Appl. Energy Mater.*, **2**, 932 (2019).
63. K. S. Novoselov, A. K. Geim, S. V. Morozov, D.-e. Jiang, Y. Zhang, S. V. Dubonos, I. V. Grigorieva and A. A. Firsov, *Science*, **306**, 666 (2004).
64. T. Gao, C. Li, Y. Wang, X. Liu, Q. An, H. N. Li, Y. Zhang, H. Cao, B. Liu and D. Wang, *Compos. Struct.*, **286**, 115232 (2022).
65. L. Peng, Y. Zhu, D. Chen, R. S. Ruoff and G. Yu, *Adv. Energy Mater.*, **6**, 1600025 (2016).
66. Z. Zhang, Y. Zhang, Y. Li, J. Lin, D. G. Truhlar and S. Huang, *Chem. Mater.*, **30**, 3208 (2018).
67. X. He, A. Tang, Y. Li, Y. Zhang, W. Chen and S. Huang, *Appl. Surf. Sci.*, **563**, 150269 (2021).
68. J. Mei, T. Liao, L. Kou and Z. Sun, *Adv. Mater.*, **29**, 1700176 (2017).
69. L. Tang, Y. Zhang, C. Li, Z. Zhou, X. Nie, Y. Chen, H. Cao, B. Liu, N. Zhang and Z. Said, *Chin. J. Mech. Eng.*, **35**, 1 (2022).
70. H. Li, Y. Zhang, C. Li, Z. Zhou, X. Nie, Y. Chen, H. Cao, B. Liu, N. Zhang and Z. Said, *Int. J. Adv. Manuf. Technol.*, **120**, 1 (2022).
71. F. Li, C. R. Cabrera and Z. Chen, *J. Mater. Chem. A*, **2**, 19180 (2014).
72. X. Zhang, Z. Yu, S.-S. Wang, S. Guan, H. Y. Yang, Y. Yao and S. A. Yang, *J. Mater. Chem. A*, **4**, 15224 (2016).
73. Z. Liu, H. Deng, S. Zhang, W. Hu and F. Gao, *J. Mater. Chem. A*, **6**, 3171 (2018).
74. X. Zhao, X. Zhang, D. Wu, H. Zhang, F. Ding and Z. Zhou, *J. Mater. Chem. A*, **4**, 16606 (2016).
75. M. Stredansky, A. Sala, T. Fontanot, R. Costantini, C. Africh, G. Comelli, L. Floreano, A. Morgante and A. Cossaro, *Chem. Commun.*, **54**, 3971 (2018).
76. S. Lin, J. Gu, H. Zhang, Y. Wang and Z. Chen, *FlatChem*, **9**, 27 (2018).
77. J. P. Perdew, K. Burke and M. Ernzerhof, *Phys. Rev. Lett.*, **77**, 3865 (1996).
78. R. A. Gaussian09, Inc., Wallingford CT 121, 150 (2009).
79. S. Grimme, *J. Comput. Chem.*, **27**, 1787 (2006).
80. S. Grimme, J. Antony, S. Ehrlich and H. Krieg, *J. Chem. Phys.*, **132**, 154104 (2010).
81. X. Yang, J. Luo and X. Sun, *Chem. Soc. Rev.*, **49**, 2140 (2020).
82. N. U. Rahman, A. A. Khan, R. Ullah, R. Ahmad and I. Ahmad, *Surf. Interfaces*, **29**, 101767 (2022).
83. H. Benzidi, M. Lakhal, M. Garara, M. Abdellaoui, A. Benyoussef and O. Mounkachi, *Phys. Chem. Chem. Phys.*, **21**, 19951 (2019).
84. B. Mortazavi, A. Dianat, O. Rahaman, G. Cuniberti and T. Rabczuk, *J. Power Sources*, **329**, 456 (2016).
85. A. Ishii, M. Yamamoto, H. Asano and K. Fujiwara, *J. Phys.: Conference Series, IOP Publishing*, 052087 (2008).
86. Y. Ding, Q. Deng, C. You, Y. Xu, J. Li and B. Xiao, *Phys. Chem. Chem. Phys.*, **22**, 21208 (2020).
87. M. Arsentev, A. Missyul, A. V. Petrov and M. Hammouri, *J. Phys. Chem. C*, **121**, 15509 (2017).
88. X.-J. Ye, G.-L. Zhu, J. Liu, C.-S. Liu and X.-H. Yan, *J. Phys. Chem. C*, **123**, 15777 (2019).
89. Y. Aierken, C. Sevik, O. Gülseren, F. M. Peeters and D. Çakır, *J. Mater. Chem. A*, **6**, 2337 (2018).
90. S. U. Rehman, A. Samad, M. Saeed, B. Amin, M. Hafeez and I. A. Mir, *Appl. Surf. Sci.*, **551**, 149304 (2021).
91. Y.-T. Du, X. Kan, F. Yang, L.-Y. Gan and U. Schwingenschlogl, *ACS Appl. Mater. Interfaces*, **10**, 32867 (2018).
92. A. Urban, D.-H. Seo and G. Ceder, *npj Comput. Mater.*, **2**, 1 (2016).
93. Z. Yang, D. Choi, S. Kerisit, K. M. Rosso, D. Wang, J. Zhang, G. Graff and J. Liu, *J. Power Sources*, **192**, 588 (2009).
94. X. Fan, J. Mao, Y. Zhu, C. Luo, L. Suo, T. Gao, F. Han, S. C. Liou and C. Wang, *Adv. Energy Mater.*, **5**, 1500174 (2015).

Supporting Information

A first-principles study of B_3O_3 monolayer as potential anode materials for calcium-ion batteries

Mustafa M. Kadhim[*,†], Ali Majdi[**], Safa K. Hachim[*,****], Sallalh. Ahmed Abdullaha[*****], Taleeb Zedan Taban[******], and Ahmed Mahdi Rheima[*******]**

*Medical Laboratory Techniques Department, Al-Farahidi University, Baghdad 10022 Iraq
**Department of Building and Construction Techniques Engineering, Al-Mustaqbal University College, 51001 Hilla, Iraq
***College of Technical Engineering, The Islamic University, Najaf, Iraq
****Medical Laboratory Techniques Department, Al-Turath University College, Iraq, Baghdad
*****The University of Mashreq, Research Center, Baghdad, Iraq
******Laser and Optoelectronics Engineering Department, Kut University College, Kut, Wasit,
*******Department of Chemistry, College of Science, Mustansiriyah University, Baghdad, Iraq
(*Received 9 August 2022 • Revised 11 October 2022 • Accepted 16 November 2022*)

Cartesian structure of B_3O_3

B	54.90000000	19.01790000	0.00000000
B	57.64500000	20.60280000	0.00000000
B	57.64500000	17.43310000	0.00000000
B	54.90000000	15.84830000	0.00000000
B	52.15500000	14.26340000	0.00000000
B	54.90000000	9.50900000	0.00000000
B	54.90000000	12.67860000	0.00000000
B	57.64500000	11.09380000	0.00000000
B	57.64500000	7.92410000	0.00000000
B	60.39000000	9.50900000	0.00000000
B	63.13500000	11.09380000	0.00000000
B	63.13500000	7.92410000	0.00000000
B	65.88000000	15.84830000	0.00000000
B	63.13500000	14.26340000	0.00000000
B	65.88000000	12.67860000	0.00000000
B	63.13500000	17.43310000	0.00000000
B	60.39000000	19.01790000	0.00000000
B	63.13500000	20.60270000	0.00000000
O	53.07000000	15.84830000	0.00000000
O	53.07000000	12.67860000	0.00000000
O	61.30500000	20.60280000	0.00000000
O	58.56000000	19.01790000	0.00000000
O	55.81500000	20.60280000	0.00000000
O	55.81500000	17.43310000	0.00000000
O	61.30500000	17.43310000	0.00000000
O	64.05000000	19.01790000	0.00000000
O	66.79500000	14.26340000	0.00000000
O	64.05000000	15.84830000	0.00000000
O	64.05000000	12.67860000	0.00000000
O	55.81500000	14.26340000	0.00000000
O	55.81500000	11.09380000	0.00000000
O	55.81500000	7.92410000	0.00000000
O	58.56000000	9.50900000	0.00000000
O	61.30500000	11.09380000	0.00000000
O	61.30500000	7.92410000	0.00000000
O	64.05000000	9.50900000	0.00000000
H	55.33499398	21.43418091	0.00000000
H	63.72497948	21.62462183	0.00000000
H	67.75500000	14.26340000	0.00000000
H	63.72500740	6.90219429	0.00000000
H	55.33499398	7.09271909	0.00000000
H	50.97500000	14.26340000	0.00000000